

Contribution of Structure and Morphology of Design Constituents to Performance Improvement of Multilayer Polaritonic Photodetector

N.L.Dmitruk^{1,*}, O.I.Mayeva¹, S.V.Mamykin¹, I.B.Mamontova¹ and O.B.Yastrubchak²

¹Institute for Physics of Semiconductors of National Academy of Sciences of Ukraine
45, Nauki av., 03028, Kyiv-28 Ukraine
FAX: +(380 44) 265-83-42

²Institute of Physics, Polish Academy of Sciences

* Author to whom correspondence should be addressed: nicola@dep39.semicond.kiev.ua

Received: 1 April 2003 / Accepted: 22 August 2003 / Published: 31 October 2003

Abstract: This paper is devoted to estimate contribution of structure and morphology of the individual design constituents to performance improvement of multilayer polaritonic photodetector (optochemical sensor). Surface plasmon resonance (SPR) in the surface barrier heterostructure (SBH) with the corrugated interface is used as the basic principle underlying the device operation. The demonstration of correlation of the contribution with the enhanced SBH features was performed through the adequate characterization tool.

Keywords: Diffraction grating, Surface plasmon resonance, Sensors devices.

Introduction

In this paper we deal with the solid-state polaritonic photodetectors based on the metal (Au,Ag,Al)/ semiconductor (GaAs, InP) surface barrier heterostructure with the periodically corrugated interface [1], which is the key element for such devices as optochemical sensor [2], selective solar cells, etc. Surface plasmon resonance in SBH with microrelief at the interface is a basic principle underlying the device operation. As with any photodetector, photon sensitivity, spectral response, selectivity

requirements, signal-to-noise ratio and durability are crucial for the SPR-based devices. Present work is intended to demonstrate improving the performance of above mentioned multilayer polaritonic photodetector. Keeping in mind the application-specific design of the SBH, structurization of each constituents of them has been adopted as the processing technique for photodetector (optical sensor) manufacturing, including sensitization - a suitably chosen treatment of intermediate layer at the interface- due to its wide opportunities for controlling sensitivity, selectivity, reliability etc. of the devices. Demonstration of the performance improvement was performed through the adequate characterization tool for multilayer systems involved.

The aim of this paper is threefold: (i) to try to obtain the deeper correlation between the surface structure and morphology of the SBH interfaces and just mentioned above photoresponsivity properties of them; (ii) to specify contribution of both structure and morphology of the individual constituents of the multilayer structures to performance of polaritonic photodetector; (iii) to maximum affect the performance by full exploitation of the advantages offered by both advanced manufacturing and treatments. In order to achieve just formulated aims, our present guidelines are: (i) for general statistical purposes, the autocorrelation function ACF $G(X)$ and the fractal analysis were used as the diagnostic instruments to describe the processes under observation, which are complementary approaches rather than competitive ones; (ii) structurizations of the SBH front covering layers; (iii) electronic sensitization of the SBH interfaces (improvement of the electrical and recombination parameters of the interface); (iv) maximizing (or optimizing) signal-to-noise ratio in the photoelectrical and optical responses of the SBH.

Samples and methods

As an advanced manufacturing of the semiconductor (GaAs, InP) surface we used such ones as some self-organized processing (anisotropic etching) to obtain quasiperiodical diffraction gratings (quasigratings), and holographic etching to receive one-dimensional diffraction gratings or cross-periodically corrugated interface (bigratings). Au, Ag and Al were chosen as a plasmon-carrying metals because of their outlook for polaritonic optoelectronic device application. Thermally evaporated thin metal films were deposited on the processed semiconductor at RT and then were (or not) annealed at 120° C. Structure variation of the top metal film of the SBH was performed by deposition of an Au island film (~100 nm) as an overlayer. Deposition of ultrathin metal layer of Cr (~3 nm) was used for better adhesion for Au. For electronic sensitization of the SBH interface, it was subjected to passivation through the hydrothermal oxidation or/and the sulfur treatment. Basic (routine) detection techniques included reflectance/ transmittance spectroscopy, spectral and angular characteristics of the SBH photoresponse, and model calculation. Advanced techniques included atomic force microscopy (AFM) and variable angle spectroscopic ellipsometry (VASE). Our interest has been focused on the statistical methods with special emphasis on characterizing the surfaces by means of fractal analysis [3]. The fractal analysis is motivated by the assumption that the real surface roughness of whole multilayer system may be superposition of a random and ordered physical processes and will possess fractal characteristics. The electrophysical parameters of the SBH (barrier height ϕ_B , nonideality factor n , density of surface states N_{ss} , recombination parameters) were deduced from I-V, C-V characteristics and from the spectral characteristics of short-circuit photocurrent j_{ph} .

Table 1. Statistical parameters for various types of surface microreliefs

Type of microrelief	Traditional surface statistics			Fractal model			
	$\sqrt{G(0)}$, nm	σ , nm	h	δ , nm	K_0 , nm ⁻¹	D	b
Quasigrating 1	215	208	0.959	214	0.00382	1.67	1.58
Grating 2	28.8	992	0.869	28.8	0.00132	1.4	1.71
Grating 3	12.8	125	0.985	12.4	0.00774	1.33	1.96
Grating 3+Al	11.7	105	1.048	11.1	0.00616	1.48	1.74
Grating 4	26.13	-	-	26.13	0.00624	1.65	1.70
Grating 4+Au	25.02	-	-	25.02	0.0060	1.71	1.68
Bigrating 5	13.7	-	-	13.2	0.0084	1.28	1.75
*Bigrating 5 ()	15.8	-	-	15.5	0.0087	1.39	1.83
*Bigrating 5 (⊥)	16.1	-	-	15.9	0.0086	1.41	1.81

*Portion of Grating 5 was subjected by repeated interferential etching in orthogonal to the grooves direction to obtain bigrating.

Results and discussion

Morphological and statistical features of the SBH

Multilayered and multidimensional (in general) texture for the frontal surface of the SBH was used. One can assume that the morphological features of the SBH are controlled by two components of the roughnesses: 1) by the roughness of the underlying surface and 2) by the roughness of the deposited film.

Measurements of the morphological and statistical features of the SBH (traditional and fractal approach) were performed with the help of processing AFM-images (Nanoscope III A, Digital Instruments, USA) using Dimension 3000 software and were provided a wide variety of statistics on textured surface, including ACF $G(X)$, rms δ , correlation length σ and fractal parameters.

AFM images of the underlying surface microreliefs obtained by the various chemical processing, their profiles and depth analysis (Fig.1) have shown that the relief received by anisotropic etching (quasigratings) on both InP and GaAs substrates are one-dimensionally rough ones, because they are a system of approximately parallel grooves oriented along the $\langle 0 \bar{0} 1 \rangle$ directions asymmetrical for the zinc blend structure. The period value of the microreliefs is increased with the rise in etching duration. Inspection of the diffraction gratings (and bigratings) to reveal morphological peculiarities of them and to determine groove depth and grating period have been performed as well. Bigrating modifications lead to formation a microtexture with the crater-like morphology on surface. For both types of the microrelief samples (quasigratings and gratings) one-argument surface autocorrelation function $G(X)$ can be considered, which are used for relief description respectively the measurements across the

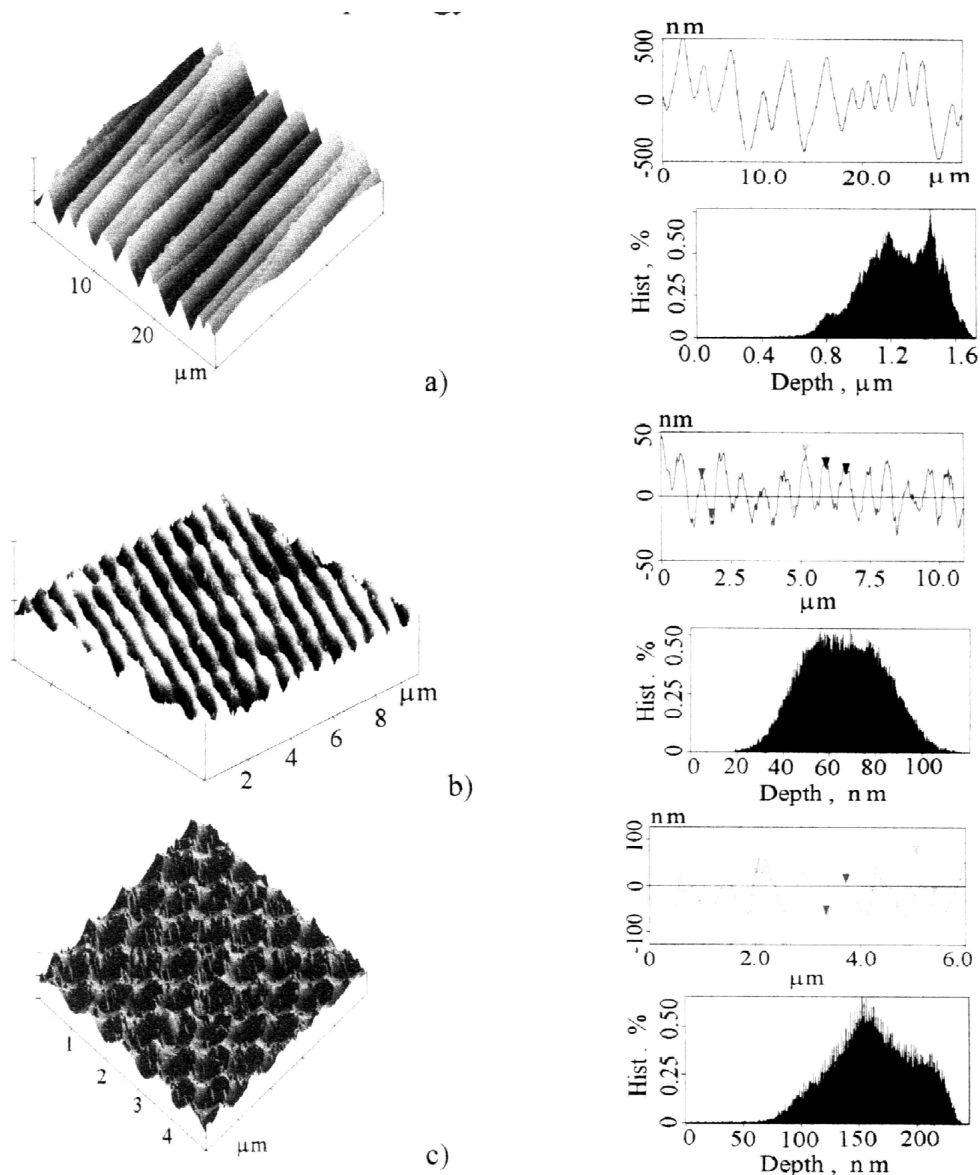


Figure 1: AFM images, section and depth analysis of microrelief surfaces of InP (a,b) and GaAs (c) with microrelief of quasigrating (a), grating (b) and bigrating (c) type. $z=1000$ nm/div (a), $z=200$ nm/div (b), $z=250$ nm/div (c).

grooves [4]; its initial portion is fairly close to Gaussian function, namely,

$$G(X) = \delta^2 \exp\left[-X/\sigma\right]^{2h} \quad (1)$$

where δ -rms and σ -correlation length and the value of the roughness exponent $h \Rightarrow 1$ for gently rounded surfaces. To model a surface with one-dimensional roughness we used the fractal function, which is expressed as a weighted sum of N periodic functions [3]:

$$G(X) = \delta^2 \sum_{n=0}^{N-1} (D-1)^{2n} \cos(K_0 b^n X), \quad (2)$$

where D ($1 < D < 2$) is the roughness fractal dimensions, K_0 is the fundamental spatial wavenumber, b

(>1) is the spatial frequency scaling parameter, and N is the number of tones.

The following results of the comparative study of the surface microreliefs are presented in Table1 and are worth noticing:

(i) A fractal model including a finite range of spatial frequencies (N=6) allows us to describe real microrelief surfaces; (ii) A real microrelief surface of the quasigrating type is more likely to be composed of a random distribution of the certain type gratings, shown in the top right-hand corner of Fig.1 (Section analysis) i.e. it is intermediate between periodic and perfectly random one. Existing some maxima in Depth analysis is characteristic of similar structures; (iii) The fractal dimension D is a measure of the roughness: the deterministic character of relief increases as the fractal dimension D decreases. The value of the spatial-frequency scaling parameter b also increases in the direction of the increase in the degree of surface order. The values of δ and $K_o = 2\pi/\Lambda_o$ (Λ_o is the main period of relief) are consistent with the AFM-images; (iv) The σ value connected with the grating 2, differs from those connected with the other gratings, but it is consistent with what could be seen on the corresponding AFM-images, namely, an inhomogeneous grating surface exhibiting large inclusions of random roughness regions as being due to doping level inhomogeneity. Those data have been reported in more detail earlier [5] but were included here for comparison; (v) Indeed, the frontal surface roughness is controlled by two components - by the roughness of the underlying surface, which can have multidimensional texture (quasi-, grating or bigrating) and by the roughness of the overlayer (Al, Au). The Al (or Au) coatings reliably replicates the grating surface: the rms δ value for the 300-A-thick Al (or for the 500-A-thick Au) film, deposited upon grating is not significantly modified the δ value obtained for grating alone. (vi) For the gratings 3 and 4 with the surface almost sinusoidal the roughness is more (similarly one as in Fig.1,b) or less gentle - $D=1.33$ and $D=1.65$, respectively, that indicates whether the higher spatial frequencies are suppressed (3) or are added (4). (vii) Data maxima on the histogram concerning bigrating AFM-image (Fig.1,c) correspond to specific depths of features on the microrelief surface - crater-like corrugation with good symmetry for bigrating thus fabricated.

The polarization and angular characteristics of the SBH

For observation of the correlation between the microrelief morphology and the light scattering features and related problems, the polarization and angular characteristics of the SBH photosensitivity in the spectral region of fundamental absorption have been measured. Fig.2 demonstrates the θ -region of j_{ph} increasing caused by enhanced local electromagnetic field due to surface plasmon excitation on quasigrating microrelief with suitable periods in accordance with conservation of momentum:

$$\sin \Theta = \left[\frac{\epsilon_1 \epsilon_2}{\epsilon_1 + \epsilon_2} \right]^{1/2} \pm m \frac{\lambda}{a}; \quad m = 1, 2, 3 \dots (3)$$

for p-polarized incident light and plane of incidence perpendicular to the quasigrating grooves or:

$$\sin \Theta = \left[\frac{\epsilon_1 \epsilon_2}{\epsilon_1 + \epsilon_2} - \left(m \frac{\lambda}{a} \right)^2 \right]^{1/2}, \quad (4)$$

for s-polarized incident light and plane of incidence parallel to the quasigrating grooves, where ϵ_1, ϵ_2 are permittivity of air and metal, respectively, and a is the suitable period of quasigrating. Because of each quasigrating is characterized by a set of parameter pairs (period and depth), so that the maxima in

Fig.2 will be somewhat broadened and attenuated. Each curve has been normalized by setting the value of function at the $\Theta=0$ to unity. The evolution from a relatively diffuse pattern with a broader maximum to the most common pattern that we have observed in VASE-regime for the typical diffraction grating with the profile close to sinusoidal. As a result, the improvement of selectivity, strongly associated with

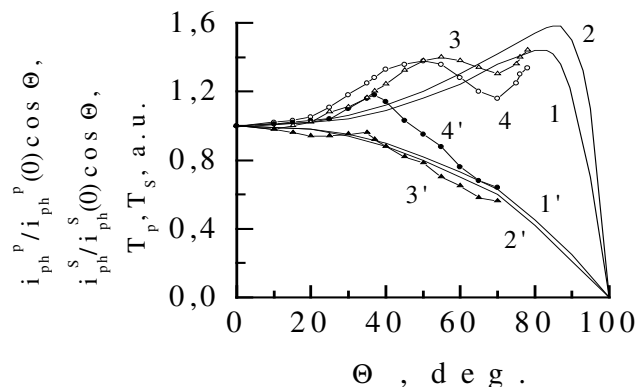


Figure 2. The calculated angular dependencies of transmittance T_p (1,2) and T_s (1',2') for the air/InP structure and experimental dependencies of photocurrent i_{ph} of Au/intrinsic oxide/n-InP SBH with microrelief of quasigrating type for light of p- (3,4) and s- (3',4') polarization with the wavelengths λ , μm : 0.55 (2,4,2',4'); 0.75 (1,3,1',3').

the optimization of geometric parameters of microreliefs involved has been received. Experimental $\psi(\lambda)$ and $\Delta(\lambda)$ curves for the Au/GaAs structures with classical grating and bigrating at the interface are plotted in Fig. 3.

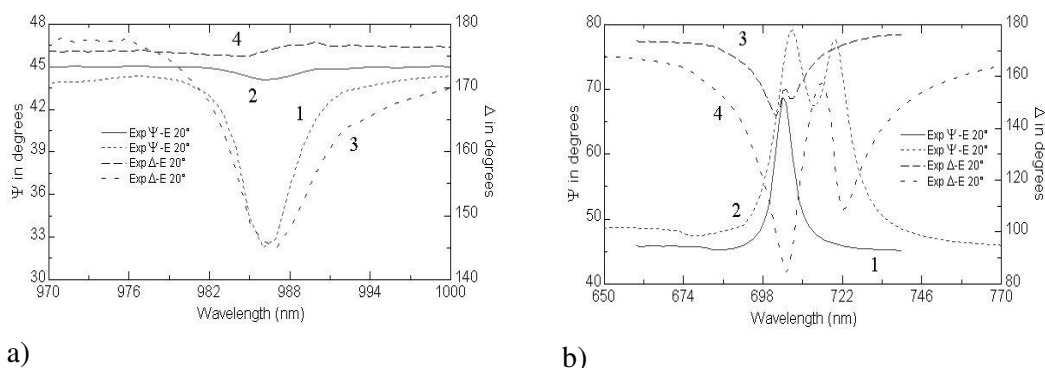


Figure 3. Experimental $\psi(\lambda)$ (1,2) and $\Delta(\lambda)$ (3,4) for Au/GaAs structures with grating (1,3) and bigrating (2,4) at the interface for p- (a) and s-polarized (b) light.

These results are consistent with the existing knowledge [6] concerning the behavior of surface plasmons on periodic metal surface, when two plasmons excited simultaneously are collinear and in opposite direction and their coupling is manifested as a splitting of the resonance peaks for s-polarized light (Fig. 3). The similar graphs for $\text{Al}_2\text{O}_3/\text{Al}/\text{GaAs}$ (grating) look much like the ones presented above. In the case of bigrating because of the interaction between two plasmon waves, the redistribution of absorption intensities between p- and s-polarizations of incident light occurs. In the

reflectance regime of measurement with the azimuth $\theta=45^\circ$ two plasmons interacting with each other are propagating in various relative directions but not in opposite directions and manifest no coupling between of yourself (or not enough to change their momenta depending strongly on the relative propagation direction of the two interaction plasmons). We will try to use there interesting peculiarities to our advantages in maximizing signal-to-noise ratio in electrical and optical devices.

Maximizing signal-to-noise ratio in the SBH

Because of the importance in maximizing signal-to-noise ratio in electric and optical devices, our special interest has been focused on reflectivity measurements **in regime of p-to-s and s-to-p conversion of light** at the diffraction grating (or bigrating) surface. By scanning the wavelength/angle of incidence for fixed angle/wavelength, using crossed polarizers between the radiation source and the photodetector, a strong resonance maximum at the surface plasmon excitation with respect to minimum background signal was achieved. The peak structures appearing in these reflection curves are symmetric about $\Theta=45^\circ$, indicating the symmetry in the surface corrugation of the bigrating. In contrast to case of classical gratings, plasmon resonances occur in the bigratings with both p- and s-polarization (Fig.4).

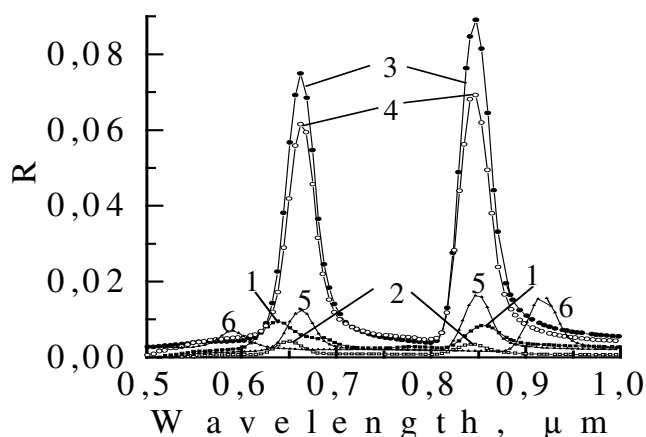


Figure 4. R_{ps} (p-to-s) (1, 3, 5, 6) and R_{sp} (s-to-p) (2, 4) conversion - experimental curves for SBH of Al/GaAs (1,2), Au/GaAs (3,4) and Au/InP (5, 6) for grating (5, 6) and bigrating (1-4). Azimuth $\Theta=45^\circ$.

Structurization of the metal films

We investigated the effects of thermal treating the Au films in attempt to find optimum both morphological and optical features needed for plasmon-carrying metal. The transmission (T) and reflection (R) data of thin gold films deposited on quartz substrates were taken and analyzed as a function of both the deposition regime and the thermal annealing conditions. These samples were surface characterized using AFM as a function of both deposition and annealing temperature.

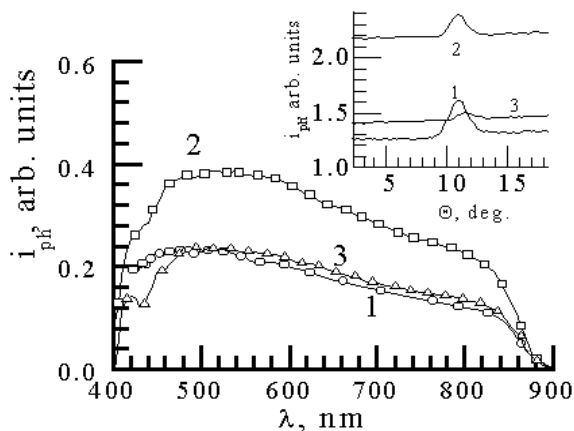


Figure 5. Spectral dependencies of short circuit photocurrent of Ag/GaAs (1) and Au/Ag/GaAs (2,3) structures with grating (period 1050 nm, modulation height 9 nm) and metal layer thicknesses: Ag- 50 nm (1); Au- 10 nm (2); 20 nm (3). Angular dependencies of i_{ph} of the same structures are shown on inset. Grating parameters were not optimized.

It was shown that at low temperature annealing ($\sim 120^\circ\text{C}$) Au films, deposited at RT, undergoes morphological transition caused by melting of small-scale irregularities and forms the optimum surface structure in view of the maximum sensitivity of the SPR photodetector. The best description of optical parameters in the connection with the microstructure of the thin Au film (microroughness, void fraction, etc.) was provided by Bruggeman EMA-model [7]. In the interest of brevity these results are not presented here.

The utilization of nanostructured island Au overlayer (Ag/Au sandwich structure) in the polaritonic SBH design was examined in conjunction with that the metal island film exhibits additional absorption band in the visible as a result of the collective oscillations of the conductive band electrons (surface or local plasmons) [8]. Then incident radiation can be coupled to plasmons, which enhances a local electromagnetic field and causes strong supplementary absorption - j_{ph} increasing. Fig.5 shows the different sensitivities of the three interfaces: the minimal (the SBH with Ag film alone as a top layer, curve 1) and the maximal (the SBH with Au/Ag bimetallic film as a top layer) ones of the SPR photodetectors: curve 2 corresponds very well to manifesting the extra features of the Au island film (overlayer), just above mentioned. Curve 3 corresponds the variation with wavelength of the short circuit photocurrent (the SBH with Au/Ag bimetal film as a top layer), where Au overlayer exhibit optical properties close to those of the bulk metal.

Electronic sensitization of the SBH

The use of different chemical processings (anisotropic etching of semiconductor, passivation of surface by oxidation or/and by sulfur treatment in an aqueous 2N solution of $\text{Na}_2\text{S}\cdot 9\text{H}_2\text{O}$) can improve electrical (surface state density) and recombination parameters of interface (diffusion length L_p , SBH barrier height ϕ_b , electron (V_n) and hole (V_p) emission rates into the metal) resulting in considerable photosensitivity enhancement. The substantial peculiarity of anisotropically etched surface is the receiving

of a controlled microrelief without formation of surface-damaged layer. The sulfur passivation of the interface have been made on the SBH photodetectors in an effort to correlate defect density at the interface with both diffusion length and other surface properties. The sulfur passivation was carried out by method [9]. Introduction of a thin intermediate layer of dielectric between the metal and the semiconductor enhances the short-wavelength sensitivity of SBH. To obtain a higher effective barrier height and lower leakage current, prior to preparing SBH photodiode the subsequent hydrothermal oxidation of InP surface was performed. A method to obtain a tunnel-thin (~6 nm) oxide layer on InP substrates with homogeneous composition was used [10]. A comparison of the SBH sensitivity with flat and chemically textured interfaces (quasigratings), presented in Fig.6, showed that there is a definite regime of an anisotroping etching which provides optimized morphology and statistical parameters result in an maximum increased SBH photosensitivity in the spectral region of fundamental absorption. The sulfidizing passivation is seen to cause a considerable photosensitivity enhancement, especially in the short-wavelength spectral region. To determine electrophysical parameters of SBH interface, the I - V characteristics were analyzed in terms of a thermoionic emission model of current transport [11]. C - V characteristics were measured as well. The interface recombination rate S/V_p , the rate of electron emission into metal V_n/D_n , and the diffusion length L_p are also determined by fitting calculated spectra of the SBH photocurrent to the experimental one taking into account the spectrum of light transition through the thin Au film into a photoactive region of the semiconductor. For thin Au film deposited onto structured substrate (grating) effective values of optical parameters are taken, following Bruggeman theory [7] (Fig.7).

Table 2. Diffusion length of holes and some parameters of SBH photodetector with diffraction grating at the interface

Samples		A, 1/mm	n	Φ_b , eV	N_{ss} , 1/cm ² eV	L_p , μm	L_p' , μm	L_p'' , μm	V_n/D_n , cm ⁻¹	S/V_p , cm ⁻¹
prior to	1	3	1.80	0.58	$2 \cdot 10^{11}$	1.8	1.7	1.7	$5.7 \cdot 10^5$	0.28
	2	0.82	2.67	0.58	-	2.9	3.1	2.9	$7 \cdot 10^4$	6.55
after S- passivation	1	3	2.19	0.57	$1.6 \cdot 10^{11}$	1.7	1.8	1.8	$5.1 \cdot 10^4$	0.34
	2	0.82	2.49	0.6	-	1.1	1.2	1.1	$6.3 \cdot 10^3$	5.17

Measurements of the diffusion length were performed under SPR condition (L_p), in off SPR (L_p'), and in s-polarized light (L_p''), A is perimeter to area ratio.

Shown in Table 2 is summary of the pertinent information for untreated and sulfidized SBH photodetector whose results are seen in Figs.6, 7. We have shown the values of effective diffusion lengths determined under various conditions (see Table) were close to each other. Some scattering data is likely caused by a locally variation in the light intensity, induced by variations of SP penetration depth. Depending upon the size of the detector, the periphery contribution may be a significant source of distortion in the electrophysical parameters determination: sulfur (S) passivation reduces the surface recombination velocity by reducing the density of the surface states and acts as confinement barrier for the minority carriers more noticeably for photodetectors with the large active area.

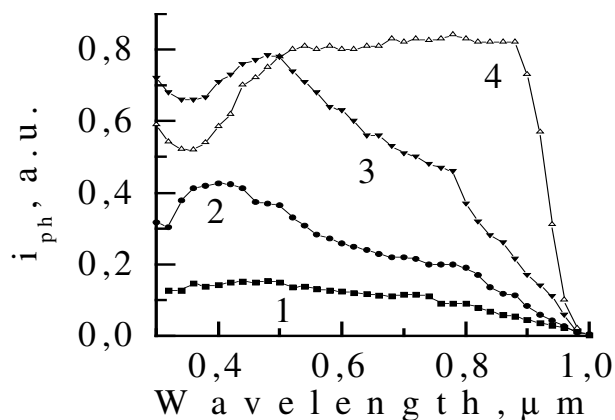


Figure 6. Photocurrent spectra i_{ph} of Au/intrinsic oxide/n-InP (100) SBH ($n=9.7 \cdot 10^{17} \text{ cm}^{-3}$) with chemically polished (1), microrelief (2-4) interfaces of quasigrating type. Duration of multistage microprofilng, min: 4 (2), 5 (3). Surface (2) subjected to oxidation followed by sulfiding is shown by curve (4).

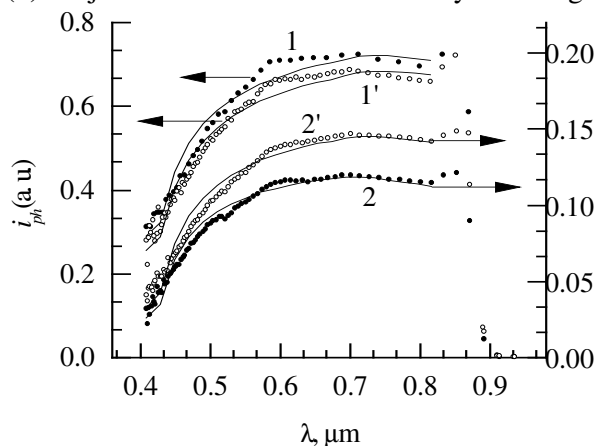


Figure 7. Experimental and calculated dependencies of short-circuit photocurrent for the Au/GaAs structures of small (1, 1') and big (2, 2') size prior to (1, 2) and after (1', 2') S-passivation.

The majority of the results manifested long-term stability (durability) of the devices in the real conditions of our laboratory.

Conclusion

Analysis of the data obtained in the collation of the fractal parameters set with the major properties of the polaritonic SBH involved have demonstrated the capability of these techniques as a promising tool for the broadening characterization of the interfaces. Simultaneously implemented these approaches should allow us: (i) to specify both critical and the most sensible factors determining efficiency of the device operation: (ii) to estimate of contribution of the structure and morphology of the individual design constituents to performance improvement of the multilayer polaritonic SBH. With the advantages of the sensitization technique used the photodetectors in UV ($S_{\lambda}=0.12\text{-}0.27 \text{ A/W}$) and visible ($S_{\lambda}=0.15\text{-}0.4 \text{ A/W}$) were elaborated in our laboratory.

Acknowledgement

This work was supported partially by the Science and Technology Center in Ukraine (project No. Uzb-56 (J)).

We would like to thank Dr. A.Kudla, Institute of Physics, Polish Academy of Sciences, for valuable help and support during the experiments.

References

1. N.Dmitruk, O.Borkovskaya, O.Mayeva, O.Fursenko, Polarization-sensitive photocurrents of metal/semiconductor structures with flat and microrelief interfaces, *Microelectron. J.* 27 (1991) 37-42.
2. N.Dmitruk, O.Mayeva, S.Mamykin, O.Yastrubchak and M.Klopfleisch, Characterization and application of multilayer diffraction gratings as optochemical sensor, *Sensors and Actuator A88* (2001) 52-57.
3. D.Jaggard, X.Sun, Scattering from fractally corrugated surfaces, *J. Opt. Soc. Am.* A7 (1990) 1131-1139.
4. N.Dmitruk, O.Mayeva, O.Yastrubcha and G.Beketov, Deterministic periodical and quasiperiodical surfaces of III-V compound: preparation, investigation and application, *Acta Phys. Polonica A* 94(1998) 285-290.
5. N.Dmitruk, O.Mayeva, O.Yastrubchak, S.Mamykin and M.Klopfleisch, Using SE to examine multilayer gratings for sensors and photodetector, Proc. of 23rd Int .Semiconds. Conf., CAS'2000 Sinaja, Romania, 2 (2000) 228-232.
6. A.Maradudin, *Surface polaritons*, ed. by V.Agranovich and D.Mills, Amsterdam, 1982, chap.10.
7. D.Bruggeman, Berechnung verschiedener physikalischer Konstanten von heterogenen Substanzen, *Ann. d. Phys.* 24 (1935) 636-679.
8. M.-L.They, Investigation of the optical properties of Au by means of thin semitransparent films, *Phys. Rev.* B2 (1970) 3061-3078.
9. J.Waldrop, Influence of S and Se on the Schottky-barrier height and interface chemistry of Au contacts to GaAs, *J. Vac. Sci. Technol.* B3 (1985) 1197-1201.
10. O.Wada, A.Majerfeld and P.Robson, InP Schottky contacts with increased barrier height, *Sol. St. Electron.* 25 (1982) 381-387.
11. O.Borkovskaya, N.Dmitruk, M.Dubovinski, R.Konakova, O.Mishchuk, and Yu.Tkhorik, The investigation of recombination properties of GaAs and its boundaries by means of photocurrent of barrier structures, *Electrotechn. Cas.* 40 (1989) 877-889.

Sample Availability: Available from the authors.